

# Control of Rectification in Molecular Junctions: Contact Effects and Molecular Signature

Quyên van Nguyen,<sup>†,||</sup> Pascal Martin,<sup>\*,†,||</sup> Denis Frath,<sup>†</sup> Maria Luisa Della Rocca,<sup>‡</sup> Frederic Lafalet,<sup>†,||</sup> Clément Barraud,<sup>‡</sup> Philippe Lafarge,<sup>‡</sup> Vineetha Mukundan,<sup>§</sup> David James,<sup>§</sup> Richard L. McCreery,<sup>§,||</sup> and Jean-Christophe Lacroix<sup>\*,†,||</sup>

<sup>†</sup>Université Paris Diderot, Sorbonne Paris Cité, ITODYS, UMR 7086 CNRS, 15 rue Jean-Antoine de Baïf, 75205 Paris Cedex 13, France

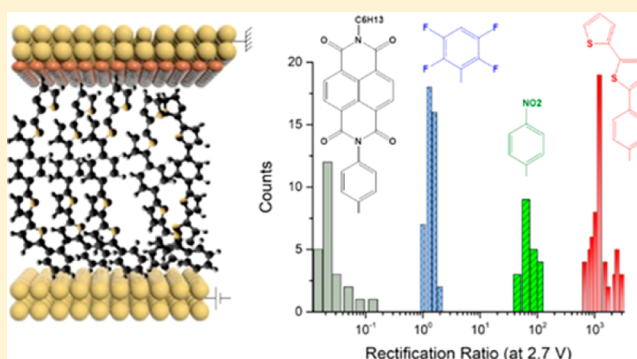
<sup>‡</sup>Laboratoire Matériaux et Phénomènes Quantiques (MPQ), Université Paris Diderot, Sorbonne Paris Cité, 75205 Paris Cedex 13, France

<sup>§</sup>University of Alberta, National Institute for Nanotechnology, 11421 Saskatchewan Drive, Edmonton, Alberta T6G 2M9, Canada

<sup>||</sup>Department of Advanced Materials Science and Nanotechnology, University of Science and Technology of Hanoi (USTH), Vietnam Academy of Science and Technology, 18 Hoang Quoc Viet, Cau Giay, Hanoi, Vietnam

## Supporting Information

**ABSTRACT:** Thin layers of oligomers with thickness between 7 and 9 nm were deposited on flat gold electrode surfaces by electrochemical reduction of diazonium reagents, then a Ti(2 nm)/Au top contact was applied to complete a solid-state molecular junction. The molecular layers investigated included donor molecules with relatively high energy HOMO, molecules with high HOMO–LUMO gaps and acceptor molecules with low energy LUMO and terminal alkyl chain. Using an oligo(bisthiénylbenzene) based layer, a molecule whose HOMO energy level in a vacuum is close to the Fermi level of the gold bottom electrode, the devices exhibit robust and highly reproducible rectification ratios above 1000 at low voltage (2.7 V). Higher current is observed when the bottom gold electrode is biased positively. When the molecular layer is based on a molecule with a high HOMO–LUMO gap, i.e., tetrafluorobenzene, no rectification is observed, while the direction of rectification is reversed if the molecular layer consists of naphthalene diimides having low LUMO energy level. Rectification persisted at low temperature (7 K), and was activationless between 7 and 100 K. The results show that rectification is induced by the asymmetric contact but is also directly affected by orbital energies of the molecular layer. A “molecular signature” on transport through layers with thicknesses above those used when direct tunneling dominates is thus clearly observed, and the rectification mechanism is discussed in terms of Fermi level pinning and electronic coupling between molecules and contacts.



## INTRODUCTION

The molecular junction (MJ) is the basic component of molecular electronics, and consists of a single molecule or an ensemble of many molecules between two conducting electrodes.<sup>1–4</sup> For molecular layers with thickness,  $d$ , below 5 nm and in many single molecule devices, direct tunneling through the molecule acting as a barrier is the dominant mechanism for transport and an exponential decrease in junction current with increasing distance is observed.<sup>4–7</sup> The attenuation factor,  $\beta$ , describing this exponential decay is in the range of 7–9 nm<sup>-1</sup> for alkane MJs, and close to 3 nm<sup>-13,4,8–10</sup> for conjugated molecules. When the thickness of the layer increases, transport is no longer consistent with direct nonresonant tunneling between the contacts and a change in  $\beta$  is often observed. It was attributed to alternative mechanism to tunneling such as activated redox “hopping”.<sup>11–14</sup> Using

bisthiénylbenzene (BTB) based molecular layers up to  $d = 22$  nm, activationless transport was observed with a  $\beta \approx 1$  nm<sup>-1</sup> at temperatures below 100 K, with high current densities (>10 A/cm<sup>2</sup>).<sup>15</sup> These results clearly indicate unusual transport mechanisms for conjugated MJs with  $d$  in the range of 5–22 nm that is above the direct tunneling limit.<sup>3</sup>

Rectification controlled by molecular structure in molecular junctions has been one of the founding proposals of Molecular Electronics.<sup>16</sup> When MJs contain a single molecular structure, either as a monolayer or as oligomers, and uses symmetric contacts, the current-density vs voltage ( $JV$ ) behavior is generally symmetric with respect to polarity, for example in Au/oligophenylimine/Au MJs<sup>17,18</sup> and a variety of aromatic

Received: June 2, 2017

Published: August 6, 2017

structures between conducting carbon electrodes.<sup>8,15,19</sup> Rectification must necessarily include an asymmetry along the transport direction.<sup>20</sup> This can be done either by using contacts based on conductive materials of different work function, or by using bilayers with a donor (D) and an acceptor (A) part in which unidirectional charge transport through the frontier molecular orbitals is favored.<sup>21–23</sup> A new design based on asymmetric anchoring moieties was also recently proposed.<sup>24</sup>

Using such systems to create rectifiers has been widely reported and recently reviewed.<sup>2</sup> Early experimental results were reported on devices incorporating hexadecyl-quinolinium tricyanoquino-dimethanide and yielded rectification ratios of 30.<sup>25,26</sup> Rectification in MJs incorporating alkane moieties bearing redox units was reported<sup>27–32</sup> but transport is limited by the high  $\beta$  value.  $A-\pi$ -D and more rarely  $A-\sigma$ -D molecules were widely used with preferred direction of the electron flow from A to D (Aviram-Ratner direction) or from D to A (reverse Aviram-Ratner direction)<sup>33,34</sup> and rectification ratio rarely exceeded 100,<sup>33–37</sup> especially for single molecule devices.<sup>21,38–41</sup> High rectification ratios were obtained using liquid mercury as a top electrode on porphyrin/fullerene bilayer devices.<sup>42</sup> High rectification ratio were also observed in alkyl-Ferrocene self-assembled monolayers, contacted by chemisorption to a bottom electrode and physisorption to a top electrode, and was shown to be strongly dependent upon the position of the Fc between the two conducting surfaces.<sup>27,29,43,44</sup> These devices are among the best molecular rectifiers to date but the techniques used to fabricate these devices suffer from the intrinsic stability limitation of the SAM-based molecular layer and EGaIn contact. Rectification as a result of asymmetric contacts<sup>24,45–47</sup> ionic screening<sup>48,49</sup> contact roughness differences<sup>50</sup> and molecular layers on silicon<sup>51–54</sup> were also reported but in each case rectification ratios remained low (i.e., below 100) or a clear molecular structural effect on rectification was not demonstrated. On a larger scale, “organic p–n diodes” composed of >100 nm thick films of organic donor and acceptor molecules<sup>55–61</sup> including the wide range of OLEDs show strong rectification behavior but the results reported here focus on much thinner molecular layers, i.e., <10 nm, which despite such ultrathin thickness exhibit high rectification ratio depending both on asymmetric contacts and molecular structure.

We have reported an Au/molecule/Ti–Au MJs structure to examine molecular layers made by diazonium electroreduction. Rectifiers were obtained when using BTB with thicknesses above 5 nm<sup>62</sup> and a 7 nm BTB film showed RR ratio over 50 while no rectification was observed with thicknesses below 5 nm.<sup>63</sup> The effect was attributed to hole injection in the BTB layer decreasing the effective tunneling barrier distance when the Au bottom electrode was positively polarized, which is similar to the mechanism proposed by Nijhuis et al. for SAM based devices incorporating ferrocene units.<sup>44</sup> The same layers when contacted by carbon show symmetric  $I(V)$  curves for film thicknesses between 2 and 22 nm.<sup>15</sup> Moreover using bilayers with overall thicknesses above 5 nm but below 22 nm control of electronic symmetry and rectification through energy level variations was recently demonstrated.<sup>64</sup> The change in transport mechanism observed above 5 nm in carbon based BTB junctions stimulated consideration of molecular layers in the Au/molecule/Ti–Au configuration with thicknesses above 5 nm, in order to develop reliable rectifiers based on a robust device design. Diazonium-based molecular junctions have proven suitable for commercial applications in electronic

music, and are compatible with massively parallel fabrication techniques.<sup>65</sup> In this thickness range with  $d > 5$  nm we also hope to demonstrate a strong “molecular signature” for the electronic response of the devices, compared to that observed when direct tunneling between the contacts is the dominant transport mechanism.

The current report describes single component MJs made by electrochemical reduction of different diazonium reagents<sup>19,64,66,67</sup> yielding layers with 7 to 9 nm thicknesses. The contacts were Au and Ti/Au, so structural asymmetry from contacts with different work function was always present in the devices studied. The molecular layers included donor molecules, namely bithienylbenzene (BTB), oligomers with relatively high energy HOMO, molecules with high HOMO–LUMO gaps (tetrafluorobenzene (FB) and nitrobenzene (NB) oligomers, and acceptor molecules, namely *n*-hexyl-naphthalenediimide (NDI) oligomers, with low energy LUMO and alkyl moieties, as shown in Figure 1a. The contacts induce asymmetry in the junction, and by varying only the composition of the layers the effects of molecular structures on  $JV$  symmetry were observed. The rectification mechanism is discussed in terms of Fermi level pinning and electronic coupling between molecules and contacts.

## EXPERIMENTAL METHODS

Unless noted otherwise, the MJs were fabricated using a gold stripe substrate on SiO<sub>2</sub>/Si wafers with width of 20  $\mu$ m and several millimeters long. The gold thickness was 45 nm on a Ti adhesion layer (2 nm). After electrochemical deposition of the organic layer, an electron beam Ti/gold top contact was deposited as described in detail previously.<sup>62,63</sup> Each sample allowed the fabrication of 16 molecular junctions with lateral dimensions of 20 by 20  $\mu$ m (area =  $4 \times 10^{-6}$  cm<sup>2</sup>). Careful control of the back pressure during Ti deposition was important, as this very reductive metal can easily be oxidized to various conductive titanium oxides.<sup>69–71</sup> A pressure of  $10^{-8}$  Torr was used to reduce oxidation from the residual oxygen and water during metal deposition, but since reaction of Ti with the organic layer cannot be excluded the molecular/Ti interface was carefully characterized using X-ray photoelectron spectroscopy (XPS). For all junctions using different molecules the Ti/Au top contact deposition was performed with identical conditions and all junctions were also completed using lithography and shadow mask for top electrode deposition. No significant differences were observed using either shadow mask or direct lithography on the molecular layer showing that the fabrication techniques used here are fully compatible with standard micro-fabrication techniques.

1-(2-Bithienyl)-4-aminobenzene and, *N*-(4-aminophenyl)-*N'*-hexylnaphthalene-1,8:4,5-tetracarboxydiimide were synthesized using procedures adapted from literature,<sup>66,68,72</sup> this last molecule being synthesized for the first time its characteristics (NMR and High Resolution Mass Spectroscopy) are given in the Supporting Information (SI files) while tetrafluoroaniline and para aminobenzene were purchased from Aldrich. Their corresponding diazonium salts were generated in situ using *tert*-butylnitrite (Aldrich) as a reagent. This procedure has been described in detail.<sup>19,66,67,73,74</sup>

Organic layer thicknesses were determined by AFM measurements. The thickness of the gold stripe deposited on SiO<sub>2</sub> was first measured using an AFM line profile. The thickness of the gold stripe covered by the grafted layer was then measured and the thickness of the organic layer was deduced by subtracting the gold thickness<sup>75</sup> using a statistical procedure as shown in Figure S1. Standard deviations of thickness were in the range of 0.4 to 0.8 nm as indicated in Table S1. Junction designations include subscripts indicating layer thicknesses in nanometers, with all devices using the same bottom and top contact electrodes. For example, Au<sub>45</sub>/BTB<sub>9</sub>/Ti<sub>2</sub>/Au<sub>45</sub> indicates a layer of 9 nm of BTB formed electrochemically on 45 nm of Au followed by 2 nm of Ti and 45 nm of Au top contact deposited in vacuum.

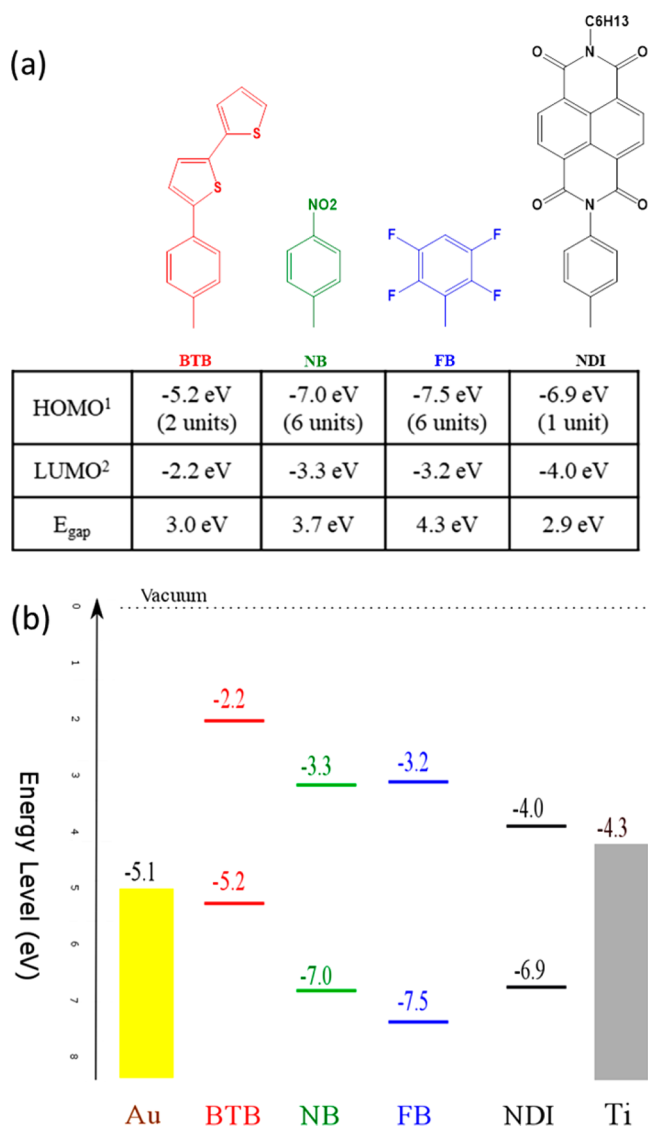


**Figure 1.** (a) Molecular unit of the oligomers used in this report with their frontier orbitals in vacuum (HOMO calculated by B3LYP/6-31G\* and LUMO deduced from UV-vis calculation (TD-DFT B3LYP/6-31G(d)) and the HOMO level. (b) Molecular orbital levels in vacuum of the various molecules and Fermi levels of the contact. Oligomer length was set to six aromatic units (phenyl or thiophene) for calculations of BTB, NB and FB, while NDI levels are for single NDI molecules since oligo(NDI) are weakly conjugated.<sup>68</sup> Note that the frontier orbital energies in vacuum neglect the mutual interaction of the oligomers as well as their interaction with the electrode.

Current density vs bias voltage ( $JV$ ) electrical characteristics of molecular junctions were measured in air with a Keithley 2602b source-meter at  $2 \text{ V s}^{-1}$  or by DC polarizing the junction while measuring the current with a low-noise current amplifier. In each case a two-probe setup configuration was used with the top electrode grounded while applying a bias to the bottom electrode. The resulting current-density/voltage ( $JV$ ) curves exhibited no hysteresis when acquired in air, or in vacuum ( $<10^{-5}$  Torr for several hours, Figure S2a). All  $JV$  curves in figures were obtained in air, and each curve presented in figures is a representative curve of  $JV$  characterization obtained with the MJs fabricated on each sample.

Low temperature measurements were performed using a variable temperature insert at a base temperature of 5 K while keeping the sample in a He atmosphere. The device was allowed to heat from 5 K to room temperature while successive  $JV$  curves were recorded.

XPS analysis was performed using Kratos AXIS XPS with Al  $K\alpha$  radiation and depth profiling with a  $4 \text{ kV Ar}^+$  beam at  $5 \times 10^{-10}$  Torr. “Blanket” samples on  $1.8 \times 1.3 \text{ cm}$  silicon surfaces covered with a pyrolyzed photoresist film.<sup>64</sup> Deposition of the BTB layer ( $d = 9 \text{ nm}$ ) was achieved using the same procedure as that for molecular junctions, and 2 nm of Ti and 20 nm of Au were deposited at  $<2 \times 10^{-7}$  Torr pressure. The thinner Au layer was required by subsequent depth profiling. Survey and high resolution spectra for C, S, O, and Ti were obtained initially and during  $\text{Ar}^+$  etching at intervals of 120 s. CasaXPS software was used for deconvolution of the XPS spectra using a Shirley baseline and Gaussian-Lorentzian line shapes.

## RESULTS

The bottom metal/BTB structure shown in Figure 2a has been described in detail previously, and consists of oligothiophene based molecules bonded by covalent bonds to the gold bottom contact.<sup>67</sup> Such layers exhibit unique on/off switching of their transport properties in an electrochemical environment. Insulating behavior is observed below 0.65 V/SCE, whereas BTB films become conductive above this potential. As a

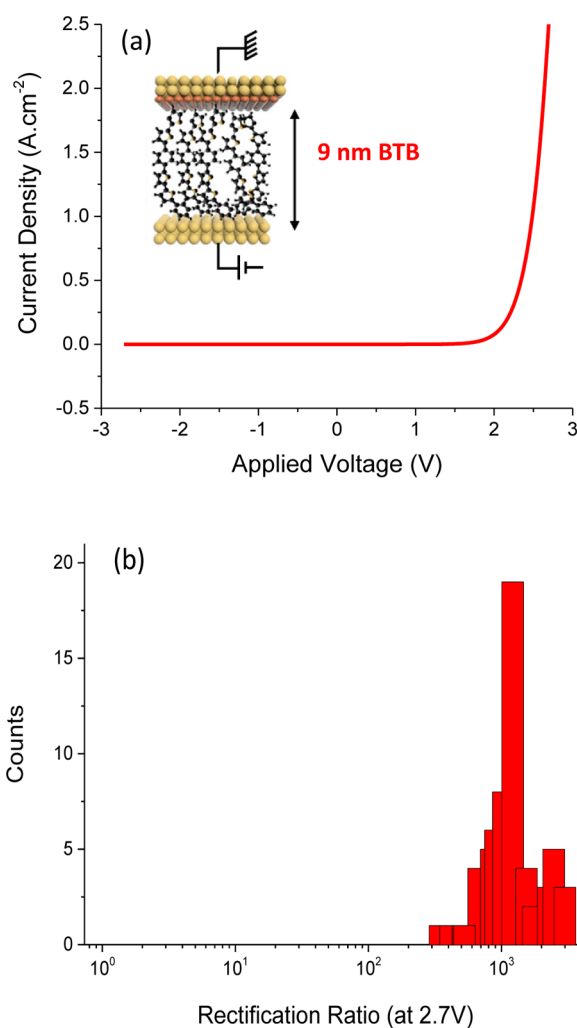


**Figure 2.** (a) Average current-density vs applied voltage ( $JV$ ) curves for Au/BTB<sub>9</sub>/Ti<sub>2</sub>/Au MJs. Inset: Schematic illustration of a molecular junction with a 9 nm thick layer of bis-thienylbenzene (BTB) grafted on a gold electrode followed by the direct deposition of a Ti(2 nm)/Au(45 nm) top electrode. Note that the number of BTB units involved in the device is more than 2. (b) Rectification Ratio ( $J(+2.7 \text{ V})/J(-2.7 \text{ V})$ ) histogram for 63 Au/BTB<sub>9</sub>/Ti<sub>2</sub>/Au junctions.

consequence, such systems combine the advantages of conductive oligomers with those of diazonium-based layers, i.e., fine control of the film thickness in the 2 to 20 nm range with robust covalent bonding. The electroactive layers with two redox states of different conductivity can be considered switchable organic electrodes.

Current-density vs. applied voltage ( $JV$ ) curves for an Au/BTB<sub>9</sub>/Ti<sub>2</sub>/Au MJ are shown in Figure 2a, for the case of ~9 nm thick films of BTB (an overlay of several  $JV$  curves collected on various junctions are given in Figure S3). As reported previously,  $JV$  curves for BTB layers between Au and Ti/Au are not symmetric with respect to polarity provided the thickness,  $d$  of the molecular layer, is greater than 5 nm. Large currents are observed when the bottom electrode is positively polarized at moderate bias whereas when negatively polarized the current flowing through the junction is much smaller. Figure S4 shows that the rectification ratio ( $RR$ ) varies with applied potential up to  $V = 2.7$  V, and Figure 2b shows histograms of the rectification ratio at +2.7 V ( $RR_{2.7V}$ ) obtained with 63 different devices produced on different samples (of the 64 junctions tested, 63 showed behavior similar to Figure 2a, for a yield of 98% when using 9 nm BTB layers). Average  $RR_{2.7V}$  is 1200 with a few devices showing  $RR_{2.7V}$  at 300 and some devices with  $RR_{2.7V}$  as high as 3000. The association of such rectification ratios to current densities as high as 2.5 A.cm<sup>-2</sup> is, to the best of our knowledge unprecedented for a single component molecular junction. These results are reproducible and devices show long-term stability (over a year). Minor dependence on scan rate from 0.1 to 100 V s<sup>-1</sup> was observed (see Figure S5). Temperature dependent measurements showed that rectification was still observed at 7 K (see Figure S2c,d,  $RR$  for BTB decreases with decreasing temperature, by a factor of 10 between 300 and 7 K, but is still large at 7 K) and transport was activation-less in the 7 to 100 K temperature range, with an Arrhenius slope <5 meV (Figure S2c) and an activation barrier of 150 meV was measured from 200 to 300 K in agreement with previous results.<sup>15</sup> These findings indicate that activation or reorganization before electron transfer are not important for transport and rectification at low temperature and exclude redox events involving titanium dioxide<sup>69,76</sup> as being the origin of the observed rectification properties.

Since similar BTB layers sandwiched between two carbon electrodes show symmetric  $JV$  curves<sup>15</sup> we can attribute at first glance the large  $RR$  ratios observed here to the use of two different metals with different work functions for contacting the BTB layer.

Ti metal can be easily oxidized to TiO<sub>2</sub> during the fabrication process, and has been previously reported to be the origin of rectification in carbon-based molecular junctions.<sup>69,76</sup> To rule out the involvement of TiO<sub>2</sub> in the rectification mechanism, we acquired XPS depth profiles during Ar<sup>+</sup> etching to yield the elemental composition of Si/SiO<sub>2</sub>/PPF/BTB<sub>9</sub>/Ti<sub>2</sub>/Au<sub>20</sub> made identically to the Au/BTB<sub>9</sub>/Ti<sub>2</sub>/Au molecular junctions but on a 1.8 × 1.3 cm area. Figure 3a shows the atomic percentages (%) vs etching time (s) of this structure before and during Ar-ion etching in the XPS chamber. At the beginning of the etching process only the Au signal is observed, as expected, but after 360 s of etching the Au signal decreases, and simultaneously carbon and titanium atomic percentages start to increase. Note that titanium and carbon signal increases before the oxygen signal, and the atomic percentage for O<sub>1s</sub> remains lower than that of titanium for all etching depths. Note

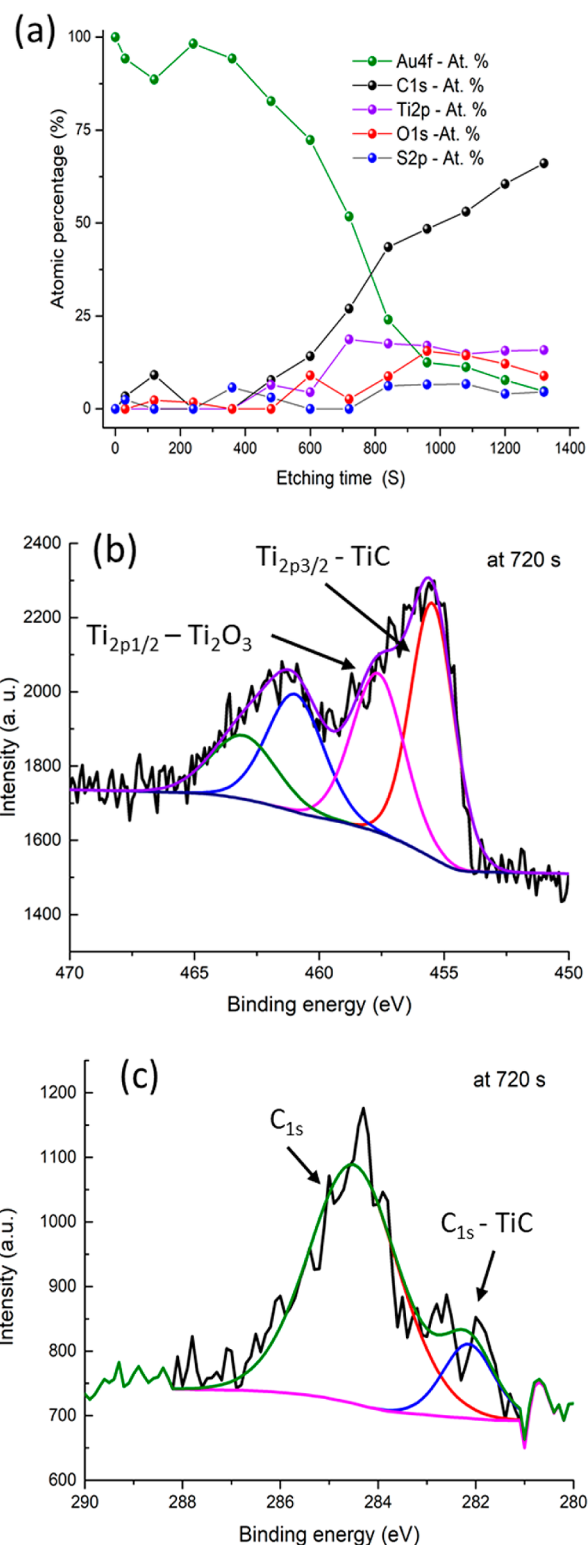


**Figure 3.** (a) Atomic percentages (%) vs etching time (s) for a Si/SiO<sub>2</sub>/PPF/BTB<sub>9</sub>/Ti<sub>2</sub>/Au<sub>20</sub> (b) titanium high resolution XPS signal, (c) carbon high resolution XPS signal.

also that the sulfur signal increases only after 700 s and that the C/S ratio reaches the theoretical value of 7 expected for a BTB layer when etching time is between 800 and 960 s. Similar experiments were performed on a Si/SiO<sub>2</sub>/PPF/Ti<sub>2</sub>/Au<sub>20</sub> large-area sample and are shown in Figure S6. In that case Au decreases and simultaneous carbon, titanium and oxygen signals

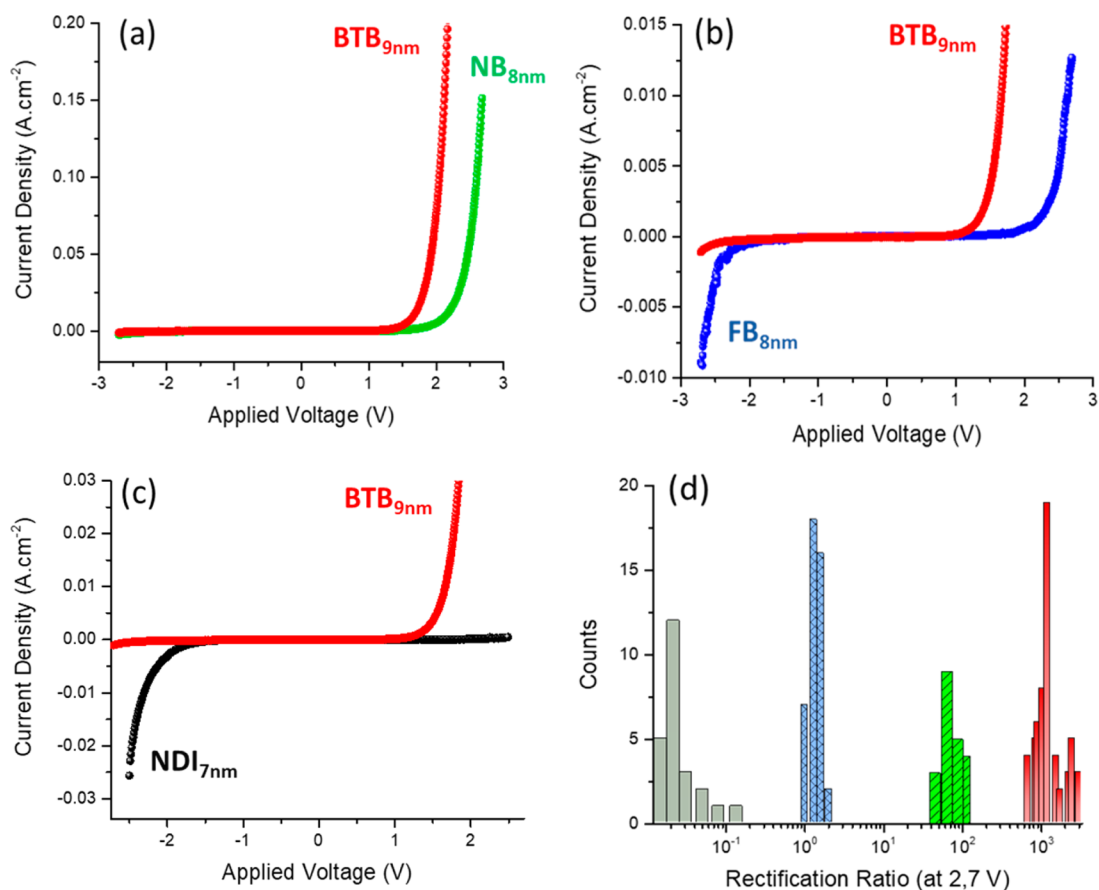


**Figure 4.** Current-density vs applied voltage ( $JV$ ) curves for (a) Au/NB<sub>8</sub>/Ti<sub>2</sub>/Au (green curve) and Au/BTB<sub>9</sub>/Ti<sub>2</sub>/Au (red curve) MJ; (b) for Au/FB<sub>8</sub>/Ti<sub>2</sub>/Au (blue curve) and Au/BTB<sub>9</sub>/Ti<sub>2</sub>/Au (red curve); (c) for Au/NDI<sub>7</sub>/Ti<sub>2</sub>/Au (gray curve) and Au/BTB<sub>9</sub>/Ti<sub>2</sub>/Au (red curve) MJ. (d) Rectification ratio  $J(+2.7\text{ V})/J(-2.7\text{ V})$  histograms for 63 BTB (red), 21 NB (green) and 42 FB (blue) devices and 26 NDI (gray) junctions.

increase (but no sulfur) are also observed with titanium atomic % being again always above that of oxygen. This excludes the formation of a 2 nm thick TiO<sub>2</sub> layer in the device, and indicates that the Ti layer is mainly Ti<sup>II</sup> and Ti<sup>III</sup> oxides, presumably mixed and disordered. Such “sub-oxides” TiO and Ti<sub>2</sub>O<sub>3</sub> contain mobile conduction band electrons and are considered metallic.<sup>69,77–79</sup> There is no evidence that the TiO<sub>x</sub> layer contains significant TiO<sub>2</sub>, and it therefore behaves like a metal rather than a large band gap semiconductor.

Figure 3b and c show the high resolution XPS spectra of the titanium and the carbon regions at 720 s etching time, at which point the oxygen signal is at its maximum. No Ti<sup>0</sup> signal at 454.0 eV is apparent in the spectra which implies nearly total reaction of the metallic Ti during deposition. No signal for the Ti<sub>2p3/2</sub> and Ti<sub>2p1/2</sub> peaks of TiO<sub>2</sub> at 459.0 and 464.7 eV are observed, but two types of titanium are present. The first one shows Ti<sub>2p3/2</sub> and Ti<sub>2p1/2</sub> at 455.5 and 460.7 eV and can be assigned to TiC or TiO species with an area of more than 60% of the total high resolution Ti 2p signal whereas the second one at 457.1 and 462.5 eV can be attributed to Ti<sub>2</sub>O<sub>3</sub>.<sup>80–83</sup> The presence of Ti–C bonds is also confirmed by the C<sub>1s</sub> signal observed at 282.1 eV (see Figure 5c) while that of carbon signal of the BTB moieties are seen at 284.3 eV.

Overall, this detailed XPS analysis clearly indicates that the Ti layer used in the BTB devices is not transformed to TiO<sub>2</sub>, and that some titanium atoms bind to the molecules and create covalent C–Ti bonds at the molecule/top electrode interface. The completed MJ is electrically equivalent to a BTB layer

between two metallic electrodes, with at least partial covalent bonding between the molecule and each electrode. The rectification observed in this work cannot be attributed to redox events involving TiO<sub>2</sub>.

The dependence of rectification on molecular structure was investigated by first replacing BTB with NB and FB (structures in Figure 1) layers of similar thicknesses. Oligo(NB) is a moiety that is less easily oxidized than oligo(BTB), with a free-molecule HOMO at –7.0 eV while that of BTB is –5.2 eV (see Figure 1). Oligo(FB) is a system with a large HOMO–LUMO gap as it is based on phenylene moieties bearing fluorine substituents. When grafted on gold by diazonium electro-reduction fluorinated oligoparaphenylenes are generated. Polyparaphenylene is known to have a band gap of 3 eV<sup>84</sup> and the presence of four fluorine groups on each benzene rings in FB will increase the bandgap further by inducing a greater degree of inter-ring torsion between adjacent phenyl units. It is thus likely that the HOMO–LUMO gap of this layer is close to that of a single AF unit and significantly above that of BTB and NB. DFT Calculations for sexi(FB) oligomer predict a HOMO at –7.5 eV and a HOMO–LUMO gap close to 4.3 eV.

Figure 4a and b compare the  $J(V)$  curves of Au/NB<sub>8</sub>/Ti<sub>2</sub>/Au (green curve) and of Au/FB<sub>8</sub>/Ti<sub>2</sub>/Au (blue curve) junctions to that of Au/BTB<sub>9</sub>/Ti<sub>2</sub>/Au (red curve). The same data are displayed as  $\ln(J$  vs  $V$ ) in Figure S7. NB and FB devices are consistently much less conductive than BTB devices as the measured current in the –2.7 V, +2.7 V potential range are smaller at all voltages. FB devices are also clearly less

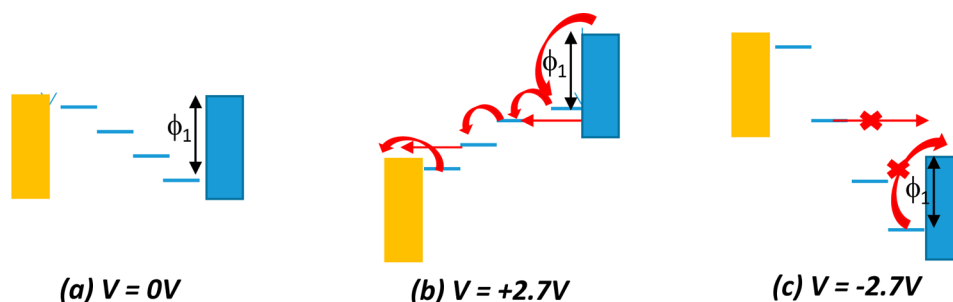


**Figure 5.** Plausible mechanism explaining the large rectification for the Au/BTB/Ti/Au devices, i.e., Energy diagram at different applied biases (a) zero, (b) positive +2.7 V, (c) negative −2.7 V. Work functions of 5.1 and 4.3 eV are assumed for a polycrystalline Au surface and a Ti surface, respectively.  $\Phi_1$  represents the initial barrier between coupled oligo(BTB) HOMO and Fermi level of TiC, whereas that between coupled oligo(BTB) HOMO and Au Fermi level is taken as close to zero for clarity. Note that the exact number of hopping steps remains unknown.

conductive than NB devices and the current scale is magnified in Figure 4b for comparison with BTB junctions. Moreover, Figure 4a shows that NB devices also rectify with a rectification ratios ( $J(+2.7\text{ V})/J(-2.7\text{ V})$ ) between 50 and 100 that is clearly lower than those observed with BTB devices. On the contrary FB devices show weak rectification behavior (RR between 1 and 3) in the bias range between −2.7 and +2.7 V. These clear variations of the current densities and rectification ratios with molecular structure are a strong indication of a molecular signature relating structure to conductance and electronic behavior when using aromatic films of 8 to 9 nm thicknesses between Au and Ti/Au electrodes.

As BTB layers consists of easily p-dopable oligomers and can be conductive above 0.6 V/SCE in an electrochemical environment, we turned to layers based on NDI, which is known to be easily reduced in an electrochemical environment (reduction potential at −0.5 and −0.7 V/SCE see Figure S8) and is an n-dopable material widely used in organic electronics. This molecule also incorporates a terminal alkyl chain that may change the electronic coupling with the top Ti/Au electrode despite covalent Ti–C bonds. Details on the grafting procedure and the characterization of the Au/NDI modified electrode used here are given in the Figure S8. As shown in Figure 1, the HOMO and LUMO energies for BTB and NDI in vacuum differ significantly, with the low LUMO energy of NDI (−4.0 eV) making it an acceptor with an energy close to the contact Fermi level of Ti or TiC.<sup>85</sup>

Figure 4c compares the  $J(V)$  curve of Au/NDI<sub>7</sub>/Ti<sub>2</sub>/Au (gray curve) to that of Au/BTB<sub>9</sub>/Ti<sub>2</sub>/Au (red curve). NDI devices are again consistently less conductive than BTB devices over the entire −2.7 V to +2.7 V potential range investigated. Importantly, the direction of rectification in the NDI device is reversed compared to that observed in BTB devices with larger  $J$  observed when the substrate bias is negative, i.e., when the potential of the Ti/Au layer is more positive than that of the Au/NDI bottom contact.

Figure 4d shows the rectification ratio ( $J(+2.7\text{ V})/J(-2.7\text{ V})$ ) histograms of more than 150 different devices (63 BTB, 21 NB and 42 FB and 25 NDI) while Figure S7d overlays the results obtained with the four different molecular layers plotted as  $\ln(J$  vs  $V$ ). The electronic behavior of the studied devices clearly depends on the molecular structure of the layers with a high level of confidence statistically. Figure 4d also makes it possible to draw several intermediate conclusions about the effect of molecular structure on  $JV$  response in single component layers contacted by Au and Ti/Au. First, single-component layers can support electron transport across molecular layer thicknesses of

9 nm, too thick to be explained by coherent tunneling between the contacts. Second, a large difference in conductance between NDI<sub>7</sub>, NB<sub>8</sub>, FB<sub>8</sub>, and BTB<sub>9</sub> (Figure 4a,b,c) is observed when such differences were not observed for different aromatic structures with thicknesses below 5 nm.<sup>19</sup> The weak effect of orbital energies on  $JV$  response when  $d < 5$  nm was attributed to strong electronic coupling between the contacts and the aromatic molecules, which causes deviation from classical Mott–Schottky behavior. This coupling induces a “leveling” effect (or “vacuum level shift”), which is known to occur at metal/organic interfaces.<sup>86–88</sup> However, above 5 nm, single-component layers of NDI, NB, FB and BTB current densities differ by orders of magnitude. This result clearly indicates that molecular structure and orbital energies have pronounced effects on  $JV$  behavior for aromatic MJs with  $d > 5$  nm and reveals that the “leveling” effect is limited to  $\sim 5$  nm from the conducting surface in aromatic devices. Third, all reported cases of single-component molecular layers between symmetric carbon contacts yielded nearly symmetric  $JV$  response, with  $RR < 2$ <sup>8,15,89</sup> while NDI<sub>7</sub> and BTB<sub>9</sub> layers between Au and Ti/Au contact are strongly asymmetric, with  $RR$  statistically below 0.01 and above 1000 respectively, i.e., with  $RR$  changing by 5 orders of magnitude. Such variations of  $RR$  with molecular structure are significantly larger than those reported in the literature.

Some mechanistic conclusions are provided below, but the experimental evidence clearly indicates that when the organic layer thickness between Au and Ti/Au contacts is large enough to avoid direct tunneling (i.e.,  $d > 5$  nm) rectification which depends strongly on molecular structure is possible for low bias voltages. Rectifying MJs can be reproducibly fabricated and their behaviors are robust due to the diazonium grafting process which bonds covalently to the bottom electrode. The rectification behavior clearly originates from the asymmetric contacts but also shows a strong dependence on molecular structure, of both rectification ratio and polarity.

As already stated, rectification must include an asymmetric feature along the transport direction. Reported examples include contacts based on conductive materials of different work function, bilayers with a donor and an acceptor part in which unidirectional charge transport is favored (Aviram–Ratner or reverse Aviram–Ratner current flow), redox groups in the layer, or layers contacted by chemisorption to the bottom electrode and physisorption to a top electrode. Since the MJ structure in the present case differs from most previous studies, several factors might contribute to the rectification mechanism. However, the current results clearly demonstrate that both

contacts and molecular structure can affect rectification and we consider several of these factors below.

The offset between the molecular orbitals and the contact Fermi level is often used to estimate the tunneling barriers for MJs and to identify the main charge carrier flowing through the device. The Fermi level of Au<sup>90</sup> is  $-5.1$  to  $-5.2$  eV vs vacuum while that of Ti and TiC is  $-4.3$  eV.<sup>85</sup> The BTB HOMO is close to the Au Fermi level and is separated from that of Ti or TiC by  $\sim 1$  eV, while the barrier between the BTB LUMO and the Fermi levels of either contact is much higher. This suggests that transport in BTB involves holes and agrees with previous reports based on transport<sup>15</sup> and photocurrents.<sup>88,91</sup> Moreover, when using BTB layers where covalent bond formation at both bottom and top electrodes is indicated experimentally, we propose that the difference in barriers for hole injection, associated with strong coupling at both electrode, is the origin of the large rectification ( $RR > 1000$ ) behavior observed for BTB based devices.

Figure 5 shows a plausible scheme explaining the rectification of BTB devices. It shows only the oligo(BTB) HOMO levels as BTB acts as a hole transporting layer and p-dopable species in electrochemical experiments.<sup>67</sup> Four HOMO levels have been arbitrarily represented as molecular relays for intrachain hopping across the 9 nm thick layer. Note that the exact number of hopping steps remains unknown and that it lies between 2 and 7 since the size of a hole in a oligo(BTB) layer is 4–5 nm and that of one BTB unit is 1.3 nm.<sup>92</sup> We assume strong coupling occurs at the Au/BTB interface due to the presence of Au–C chemical bonds and the BTB HOMO being close to the Au Fermi level, and therefore hole injection at this interface is near resonance with a small barrier. In other words, we can assume that part of the BTB layer acts as an extended electrode with almost no barrier for hole injection at the Au/BTB interface.<sup>62</sup> The presence of TiC at the BTB/Ti/Au top interface also leads to strong coupling but the initial barrier for hole injection at this interface is much higher. As a consequence Fermi level pinning is expected at both interfaces and the difference in work function between Au and TiC generates the energy scheme depicted in Figure 5a at zero bias with the four BTB HOMO levels decreasing in energy from the gold to the titanium electrode. The barrier between the BTB HOMO and Ti, noted  $\Phi_1$  in Figure 5 is significantly larger than that between BTB and Au. Since the barrier for hole formation in BTB at the Au/BTB interface is smaller than the barrier at the TiC electrode, we expect holes to form in BTB HOMO levels under positive bias. Once these holes are created it is possible for the TiC electrode to compensate the resulting positive charge by injecting electrons into the emptied HOMOs of the oligomers. Note that transport can be obtained by tunneling from a molecular state in resonance with the Fermi level of the electrode (straight arrows) but also by activated processes depicted in Figure 5b by curved arrows. When the bias is reversed as in Figure 5c, hole injection from the BTB layer into Ti is energetically much less favorable for two reasons. First, the applied bias has to compensate for the initial ( $\Phi_1$ ) barrier located at the BTB/TiC interface. Second, tunneling from a molecular state of an oligoBTB moiety in resonance with an empty level in the electrode will be slower because of a larger tunneling distance. As a consequence, at  $-2.7$  V little current crosses the devices as depicted in Figure 5c. As Fermi level pinning occurs at BTB/TiC interface, decreasing  $\Phi_1$  is difficult and needs to reach bias above  $-2.7$  V to allow the coupled HOMO of oligo(BTB) at the BTB/TiC interface to rise close

to the Fermi level of titanium, and participate in charge transport. Moreover, a bias above 2.7 V will also be needed to allow a molecular state with small enough tunneling distance to reach resonance with the Fermi level of the titanium electrode.

This proposed mechanism involving strong electronic coupling and Fermi level pinning at both interfaces can reasonably rationalize the large rectification observed for BTB. Note that this mechanism explains also easily the temperature dependence of the current observed at positive or negative bias (see Figure S2). Indeed, for positive bias, the thermally activated current observed between 100 and 290 K with low activation energy of 150 meV can be attributed to the small barrier at the Au/BTB interface. For negative bias no observable activation in the same temperature range was observed as a result of the large barrier at the BTB/TiC interface. It also predicts that the RR ratio in BTB devices is mainly linked to the initial barrier and to the Fermi level pinning at the BTB/TiC interface of the top contact. Decreasing this barrier or the Fermi level pinning at this interface, by any means, should decrease the RR observed. Figure S9 shows an extreme case in which electronic coupling is negligible at the top electrode as if the layer were studied using STM with Ti tip. In that case, it is easier to compensate for the initial ( $\Phi_1$ ) barrier located at the weakly coupled BTB/Ti interface by applying negative bias which decreases sharply the rectification ratio. The situation shown in Figure 5b is also consistent with a preferential current flow for positive bias with NB, i.e., in the same direction as that observed with BTB (see Figure S10) and a smaller RR observed for FB. In the former case, transport likely involves electrons and the barrier for electron injection is smaller at the NB/Ti interface. Assuming strong coupling at both electrodes, this results in a preferential current flow in the same direction as that observed in BTB. Furthermore; as these barriers are higher compared to those with BTB, NB devices are less conductive and the differences in barriers for electron injection have less effect on RR. In the latter case (FB), the high HOMO–LUMO gap creates significant barriers at both interfaces, thus decreasing again  $J$  and RR.

It is however not possible using this mechanism to explain the reversal of rectification polarity for NDI-based devices. The NDI LUMO is only 0.3 V above the Fermi level of Ti and TiC while its HOMO is 2 V below that of gold which suggests that transport mainly involves electron injection in NDI MJs with molecular layer thicknesses above the direct tunneling limit between the two electrodes. This is confirmed by photocurrent experiments on NDI junctions which are consistent with LUMO mediation.<sup>91</sup> This injection will be much easier at the NDI/Ti interface as depicted in Figure 1b so that if electronic coupling is similar at both electrodes, current will be stronger for positive bias, i.e., in the same direction as that observed in BTB devices. This is clearly not observed here as electrons are experimentally more easily injected in the NDI layer at negative bias, i.e., when the Au bottom electrode is negative and Ti/Au top electrode is positive. As a consequence, we propose that the direction of the rectification observed with NDI-based devices can be explained if the couplings of the molecular layer with the contacts are not the same as those demonstrated in BTB-based devices, despite the identical conditions used for fabrication of the devices. One plausible explanation is that weak coupling occurs at the bottom Au/NDI interface as a result of a LUMO localized (see Figure S11) on the central part of the NDI molecule and a large energy difference between the NDI

LUMO and the Fermi level of Au. It is also possible that NDI is less strongly coupled at the Ti interface compared to BTB due to the long alkyl moiety which is known to induce a decoupling effect.<sup>93</sup> Assuming such a situation, higher current can be obtained when the device is negatively biased depending on the relative coupling strength at each electrode as recently demonstrated in single molecule junctions.<sup>94</sup> More complex scenarios can also be considered as molecular resonance between HOMO and LUMO orbitals inside a molecular chain leading to bipolar transport.<sup>95</sup> Full explanation of the mechanism behind rectification in NDI-based devices is beyond the scope of this work and experiments including XPS depth profile and varying the length of the alkyls moieties will be reported elsewhere. Moreover, a full understanding of the rectification mechanism discussed in this study may be achieved by state of the art theoretical modeling that includes the entire system using a nonequilibrium Green's functions (NEGF) approach.<sup>46,96</sup>

## CONCLUSIONS

Molecular junctions with thicknesses between 7 and 9 nm using two contacts of different work function exhibit significant changes in electronic behavior with variation of structure of the molecular layer. Using oligo(bisthienylbenzene), a molecule whose HOMO energy level in a vacuum is close to the Fermi level of the gold bottom electrode, the devices exhibit robust and highly reproducible rectification ratios above 1000 at low voltage (2.7 V). Higher current is observed when the bottom gold electrode is biased positively and Ti/Au is negative. When the molecular layer is based on a molecule with high HOMO–LUMO gap, i.e., tetrafluorobenzene, no rectification is observed while the direction of rectification is reversed if the molecular layer consists of molecules with low LUMO energy level, i.e., naphthalene diimides with alkyl moieties. Rectification persisted at very low temperature (7 K), and was activationless between 7 and 100 K. The results show that rectification is induced by the asymmetric contacts but is also directly affected by orbital energies of the molecular layer. A “molecular signature” relating structure to transport through layers with thicknesses above those used when direct tunneling dominates is thus clearly observed, and RR variation by 5 orders of magnitude is demonstrated in this regime. The rectification mechanism is discussed in terms of electronic coupling between molecules and contacts and can be understood if one considers that such coupling depends on the molecular layer structure, since the same fabrication process has been used for all studied junctions. These observations clearly demonstrate a rectifying molecular junction can be “designed” by controlling the HOMO and LUMO energies as well as the electronic coupling at the interfaces.

## ASSOCIATED CONTENT

### Supporting Information

The Supporting Information is available free of charge on the ACS Publications website at DOI: 10.1021/jacs.7b05732.

Synthesis of NDI compound, electrochemical reduction conditions, determination of molecular layer thickness by AFM, temperature dependence measurement of Au/BTB<sub>9 nm</sub>/Ti<sub>2 nm</sub>/Au device, Overlaid JV curves of several MJs devices, Rectification ratio vs applied Voltage, Scan rate dependence on Au/BTB<sub>9 nm</sub>/Ti/Au MJs, Atomic percentages vs Etching time (s) for a Si/SiO<sub>2</sub>/PPF/Ti<sub>2</sub>/

Au<sub>20</sub> Ln J vs V curves of BTB, NDI, FB, NB molecule junctions, electroactivity of NDI modified carbon electrode, energetic diagram and plausible mechanism assuming electronic coupling is negligible at the top electrode, LUMO shape of NDI molecules (PDF)

## AUTHOR INFORMATION

### Corresponding Authors

\*E-mail: pascal.martin@univ-paris-diderot.fr.

\*E-mail: lacroix@univ-paris-diderot.fr.

### ORCID

Pascal Martin: 0000-0003-1010-8421

Frederic Lafolet: 0000-0001-6313-2308

Richard L. McCreery: 0000-0002-1320-4331

Jean-Christophe Lacroix: 0000-0002-7024-4452

### Notes

The authors declare no competing financial interest.

## ACKNOWLEDGMENTS

This work was supported the French Agence Nationale de la Recherche under Grant ANR-15-CE09 0001-01) and by the University of Alberta, the National Research Council of Canada, the National Science and Engineering Research Council and Alberta Innovates.

## REFERENCES

- (1) Xiang, D.; Wang, X.; Jia, C.; Lee, T.; Guo, X. *Chem. Rev.* **2016**, *116*, 4318–4440.
- (2) Metzger, R. M. *Chem. Rev.* **2015**, *115*, 5056–5115.
- (3) McCreery, R. L.; Yan, H.; Bergren, A. J. *Phys. Chem. Chem. Phys.* **2013**, *15*, 1065–1081.
- (4) Vilan, A.; Aswal, D.; Cahen, D. *Chem. Rev.* **2017**, *117*, 4248–4286.
- (5) Yoon, H. J.; Shapiro, N. D.; Park, K. M.; Thuo, M. M.; Soh, S.; Whitesides, G. M. *Angew. Chem., Int. Ed.* **2012**, *51*, 4658–4661.
- (6) Tran, E.; Duati, M.; Mullen, K.; Zharnikov, M.; Whitesides, G. M.; Rampi, M. *Adv. Mater.* **2006**, *18*, 1323.
- (7) Li, C.; Pobelov, I.; Wandlowski, T.; Bagrets, A.; Arnold, A.; Evers, F. *J. Am. Chem. Soc.* **2008**, *130*, 318–326.
- (8) Bergren, A. J.; McCreery, R. L.; Stoyanov, S. R.; Gusarov, S.; Kovalenko, A. J. *Phys. Chem. C* **2010**, *114*, 15806–15815.
- (9) He, J.; Chen, F.; Li, J.; Sankey, O. F.; Terazono, Y.; Herrero, C.; Gust, D.; Moore, T. A.; Moore, A. L.; Lindsay, S. M. *J. Am. Chem. Soc.* **2005**, *127*, 1384–1385.
- (10) Capozzi, B.; Dell, E. J.; Berkelbach, T. C.; Reichman, D. R.; Venkataraman, L.; Campos, L. M. *J. Am. Chem. Soc.* **2014**, *136*, 10486–10492.
- (11) Choi, S. H.; Kim, B.; Frisbie, C. D. *Science* **2008**, *320*, 1482–1486.
- (12) Luo, L.; Choi, S. H.; Frisbie, C. D. *Chem. Mater.* **2011**, *23*, 631–645.
- (13) Choi, S. H.; Risko, C.; Delgado, M. C. R.; Kim, B.; Bredas, J.-L.; Frisbie, C. D. *J. Am. Chem. Soc.* **2010**, *132*, 4358–4368.
- (14) Hines, T.; Diez-Perez, I.; Hihath, J.; Liu, H.; Wang, Z.-S.; Zhao, J.; Zhou, G.; Müllen, K.; Tao, N. *J. Am. Chem. Soc.* **2010**, *132*, 11658–11664.
- (15) Yan, H.; Bergren, A. J.; McCreery, R.; Della Rocca, M. L.; Martin, P.; Lafarge, P.; Lacroix, J. C. *Proc. Natl. Acad. Sci. U. S. A.* **2013**, *110*, 5326–5330.
- (16) Aviram, A.; Ratner, M. *Chem. Phys. Lett.* **1974**, *29*, 277–283.
- (17) Xie, Z.; Bâldea, I.; Smith, C. E.; Wu, Y.; Frisbie, C. D. *ACS Nano* **2015**, *9*, 8022–8036.
- (18) Kim, B.; Choi, S. H.; Zhu, X. Y.; Frisbie, C. D. *J. Am. Chem. Soc.* **2011**, *133*, 19864–19877.

- (19) Sayed, S. Y.; Fereiro, J. A.; Yan, H.; McCreery, R. L.; Bergren, A. *J. Proc. Natl. Acad. Sci. U. S. A.* **2012**, *109*, 11498–11503.
- (20) Mujica, V.; Ratner, M. A.; Nitzan, A. *Chem. Phys.* **2002**, *281*, 147–150.
- (21) Elbing, M.; Ochs, R.; Koentopp, M.; Fischer, M.; von Hänisch, C.; Weigend, F.; Evers, F.; Weber, H. B.; Mayor, M. *Proc. Natl. Acad. Sci. U. S. A.* **2005**, *102*, 8815–8820.
- (22) Stadler, R.; Geskin, V.; Cornil, J. *J. Phys.: Condens. Matter* **2008**, *20*, 374105.
- (23) Berlin, Y. A.; Grozema, F. C.; Siebbeles, L. D. A.; Ratner, M. A. *J. Phys. Chem. C* **2008**, *112*, 10988–11000.
- (24) Van Dyck, C.; Ratner, M. A. *Nano Lett.* **2015**, *15*, 1577–1584.
- (25) Metzger, R. M.; Chen, B.; Höpfner, U.; Lakshmikantham, M. V.; Vuillaume, D.; Kawai, T.; Wu, X.; Tachibana, H.; Hughes, T. V.; Sakurai, H.; Baldwin, J. W.; Hosch, C.; Cava, M. P.; Brehmer, L.; Ashwell, G. J. *J. Am. Chem. Soc.* **1997**, *119*, 10455–10466.
- (26) Vuillaume, D.; Chen, B.; Metzger, R. M. *Langmuir* **1999**, *15*, 4011–4017.
- (27) Nijhuis, C. A.; Reus, W. F.; Whitesides, G. M. *J. Am. Chem. Soc.* **2009**, *131*, 17814–17827.
- (28) Yuan, L.; Breuer, R.; Jiang, L.; Schmittel, M.; Nijhuis, C. A. *Nano Lett.* **2015**, *15*, 5506–5512.
- (29) Yuan, L.; Nerngchamnon, N.; Cao, L.; Hamoudi, H.; del Barco, E.; Roemer, M.; Sriramula, R. K.; Thompson, D.; Nijhuis, C. A. *Nat. Commun.* **2015**, *6*, 7324.
- (30) Chabiny, M. L.; Chen, X.; Holmlin, R.; Jacobs, H.; Skulason, H.; Frisbie, C. D.; Mujica, V.; Ratner, M.; Rampi, M. A.; Whitesides, G. M. *J. Am. Chem. Soc.* **2002**, *124*, 11730–11736.
- (31) Trasobares, J.; Vuillaume, D.; Théron, D.; Clément, N. *Nat. Commun.* **2016**, *7*, 12850.
- (32) Souto, M.; Yuan, L.; Morales, D. C.; Jiang, L.; Ratera, I.; Nijhuis, C. A.; Veciana, J. *J. Am. Chem. Soc.* **2017**, *139*, 4262–4265.
- (33) Metzger, R. M. *Chem. Phys.* **2006**, *326*, 176–187.
- (34) Metzger, R. M.; Mattern, D. L. In *Unimolecular and Supramolecular Electronics II: Chemistry and Physics Meet at Metal-Molecule Interfaces*; Metzger, R. M., Ed.; Springer: Berlin Heidelberg, 2012; pp 39–84.
- (35) Lenfant, S.; Krzeminski, C.; Delerue, C.; Allan, G.; Vuillaume, D. *Nano Lett.* **2003**, *3*, 741–746.
- (36) Meany, J. E.; Johnson, M. S.; Woski, S. A.; Metzger, R. M. *ChemPlusChem* **2016**, *81*, 1152–1155.
- (37) Johnson, M. S.; Kota, R.; Mattern, D. L.; Metzger, R. M. *Langmuir* **2016**, *32*, 6851–6859.
- (38) Hihath, J.; Bruot, C.; Nakamura, H.; Asai, Y.; Díez-Pérez, I.; Lee, Y.; Yu, L.; Tao, N. *ACS Nano* **2011**, *5*, 8331–8339.
- (39) Díez-Pérez, I.; Hihath, J.; Lee, Y.; Yu, L.; Adamska, L.; Kozhushner, M. A.; Oleynik, I. I.; Tao, N. *Nat. Chem.* **2009**, *1*, 635–641.
- (40) Batra, A.; Darancet, P.; Chen, Q.; Meisner, J. S.; Widawsky, J. R.; Neaton, J. B.; Nuckolls, C.; Venkataraman, L. *Nano Lett.* **2013**, *13*, 6233–6237.
- (41) Lee, Y.; Carsten, B.; Yu, L. *Langmuir* **2009**, *25*, 1495–1499.
- (42) Koiry, S. P.; Jha, P.; Aswal, D. K.; Nayak, S. K.; Majumdar, C.; Chattopadhyay, S.; Gupta, S. K.; Yakhmi, J. V. *Chem. Phys. Lett.* **2010**, *485*, 137–141.
- (43) Nijhuis, C. A.; Reus, W. F.; Siegel, A. C.; Whitesides, G. M. *J. Am. Chem. Soc.* **2011**, *133*, 15397–15411.
- (44) Nijhuis, C. A.; Reus, W. F.; Whitesides, G. M. *J. Am. Chem. Soc.* **2010**, *132*, 18386–18401.
- (45) Kuikka, M. A.; Li, W.; Kavanagh, K. L.; Yu, H.-Z. *J. Phys. Chem. C* **2008**, *112*, 9081–9088.
- (46) Zhao, J.; Yu, C.; Wang, N.; Liu, H. *J. Phys. Chem. C* **2010**, *114*, 4135–4141.
- (47) Vezzoli, A.; Brooke, R. J.; Ferri, N.; Higgins, S. J.; Schwarzacher, W.; Nichols, R. J. *Nano Lett.* **2017**, *17*, 1109–1115.
- (48) Capozzi, B.; Xia, J.; Adak, O.; Dell, E. J.; Liu, Z.-F.; Taylor, J. C.; Neaton, J. B.; Campos, L. M.; Venkataraman, L. *Nat. Nanotechnol.* **2015**, *10*, 522–527.
- (49) Zhang, W.; Zhang, X.; Lu, C.; Wang, Y.; Deng, Y. *J. Phys. Chem. C* **2012**, *116*, 9227–9234.
- (50) Jin, Y.; Friedman, N.; Sheves, M.; Cahen, D. *Langmuir* **2008**, *24*, 5622–5626.
- (51) Li, Y.; Calder, S.; Yaffe, O.; Cahen, D.; Haick, H.; Kronik, L.; Zuilhof, H. *Langmuir* **2012**, *28*, 9920–9929.
- (52) Popoff, R. T. W.; Zavareh, A. A.; Kavanagh, K. L.; Yu, H.-Z. *J. Phys. Chem. C* **2012**, *116*, 17040–17047.
- (53) Yu, X.; Lovrinčić, R.; Kraynis, O.; Man, G.; Ely, T.; Zohar, A.; Toledano, T.; Cahen, D.; Vilan, A. *Small* **2014**, *10*, S151–S160.
- (54) Zhu, L.; Popoff, R. T. W.; Yu, H.-Z. *J. Phys. Chem. C* **2015**, *119*, 1826–1831.
- (55) Kleemann, H.; Gutierrez, R.; Avdoshenko, S.; Cuniberti, G.; Leo, K.; Lüssem, B. *Org. Electron.* **2013**, *14*, 193–199.
- (56) Kleemann, H.; Gutierrez, R.; Lindner, F.; Avdoshenko, S.; Manrique, P. D.; Lüssem, B.; Cuniberti, G.; Leo, K. *Nano Lett.* **2010**, *10*, 4929–4934.
- (57) Sengoku, T.; Yamao, T.; Hotta, S. *J. Non-Cryst. Solids* **2012**, *358*, 2525–2529.
- (58) Saracco, E.; Bouthinon, B.; Verilhac, J.-M.; Celle, C.; Chevalier, N.; Mariolle, D.; Dhez, O.; Simonato, J.-P. *Adv. Mater.* **2013**, *25*, 6534–6538.
- (59) Kong, H.; Sinha, J.; Hoeft, D.; Kirschner, S. B.; Reich, D. H.; Katz, H. E. *Org. Electron.* **2013**, *14*, 703–710.
- (60) Gong, X.; Tong, M.; Xia, Y.; Cai, W.; Moon, J. S.; Cao, Y.; Yu, G.; Shieh, C.-L.; Nilsson, B.; Heeger, A. J. *Science* **2009**, *325*, 1665–1667.
- (61) He, S. J.; White, R.; Wang, D. K.; Zhang, J.; Jiang, N.; Lu, Z. H. *Org. Electron.* **2014**, *15*, 3370–3374.
- (62) Martin, P.; Della Rocca, M. L.; Anthore, A.; Lafarge, P.; Lacroix, J.-C. *J. Am. Chem. Soc.* **2012**, *134*, 154–157.
- (63) Fluteau, T.; Bessis, C.; Barraud, C.; Della Rocca, M. L.; Martin, P.; Lacroix, J.-C.; Lafarge, P. *J. Appl. Phys.* **2014**, *116*, 114509.
- (64) Bayat, A.; Lacroix, J.-C.; McCreery, R. L. *J. Am. Chem. Soc.* **2016**, *138*, 12287–12296.
- (65) Bergren, A. J.; Zeer-Wanklyn, L.; Semple, M.; Pekas, N.; Szeto, B.; McCreery, R. L. *J. Phys.: Condens. Matter* **2016**, *28*, 094011.
- (66) Fave, C.; Leroux, Y.; Trippé, G.; Randriamahazaka, H.; Noel, V.; Lacroix, J.-C. *J. Am. Chem. Soc.* **2007**, *129*, 1890–1891.
- (67) Fave, C.; Noel, V.; Ghilane, J.; Trippé-Allard, G.; Randriamahazaka, H.; Lacroix, J. C. *J. Phys. Chem. C* **2008**, *112*, 18638–18643.
- (68) Kobaisi, M. A.; Bhosale, S. V.; Latham, K.; Raynor, A. M.; Bhosale, S. V. *Chem. Rev.* **2016**, *116*, 11685–11796.
- (69) Wu, J.; McCreery, R. L. *J. Electrochem. Soc.* **2009**, *156*, P29–P37.
- (70) Nowak, A. M.; McCreery, R. L. *J. Am. Chem. Soc.* **2004**, *126*, 16621–16631.
- (71) McCreery, R. L.; Wu, J.; Prasad Kalakodimi, R. *Phys. Chem. Chem. Phys.* **2006**, *8*, 2572–2590.
- (72) Hayes, R. T.; Wasielewski, M. R.; Gosztola, D. *J. Am. Chem. Soc.* **2000**, *122*, 5563–5567.
- (73) Stockhausen, V.; Trippé-Allard, G.; Van Quynh, N.; Ghilane, J.; Lacroix, J.-C. *J. Phys. Chem. C* **2015**, *119*, 19218–19227.
- (74) Stockhausen, V.; Ghilane, J.; Martin, P.; Trippé-Allard, G.; Randriamahazaka, H.; Lacroix, J.-C. *J. Am. Chem. Soc.* **2009**, *131*, 14920–14927.
- (75) Stockhausen, V.; Nguyen, V. Q.; Martin, P.; Lacroix, J. C. *ACS Appl. Mater. Interfaces* **2017**, *9*, 610–617.
- (76) Wu, J.; Mobley, K.; McCreery, R. L. *J. Chem. Phys.* **2007**, *126*, 024704.
- (77) Grigorov, K. G.; Grigorov, G. I.; Drajeva, L.; Bouchier, D.; Sporken, R.; Caudano, R. *Vacuum* **1998**, *51*, 153–155.
- (78) Bartholomew, R. F.; Frankl, D. R. *Phys. Rev.* **1969**, *187*, 828–833.
- (79) Strachan, J. P.; Pickett, M. D.; Yang, J. J.; Aloni, S.; David Kilcoyne, A. L.; Medeiros-Ribeiro, G.; Stanley Williams, R. *Adv. Mater.* **2010**, *22*, 3573–3577.
- (80) Ottakam Thotiyil, M. M.; Freunberger, S. A.; Peng, Z.; Chen, Y.; Liu, Z.; Bruce, P. G. *Nat. Mater.* **2013**, *12*, 1050–1056.

- (81) Restrepo Parra, E.; Arango Arango, P. J.; Benavides Palacio, V. J. *DYNA* **2010**, *77*, 64–74.
- (82) Johansson, L. I.; Hagström, A. L.; Jacobson, B. E.; Hagström, S. B. M. *J. Electron Spectrosc. Relat. Phenom.* **1977**, *10*, 259–271.
- (83) Blackstock, J. J.; Donley, C. L.; Stickle, W. F.; Ohlberg, D. A. A.; Yang, J. J.; Stewart, D. R.; Williams, R. S. *J. Am. Chem. Soc.* **2008**, *130*, 4041–4047.
- (84) Lacaze, P. C.; Aeiyaich, S.; Lacroix, J. C. In *Handbook of Organic Conductive Molecules and Polymers*; Nalwa, H. S., Ed.; Wiley: New York, 1997; Vol. 2, pp 205–264.
- (85) Santerre, F.; El Khakani, M. A.; Chaker, M.; Dodelet, J. P. *Appl. Surf. Sci.* **1999**, *148*, 24–33.
- (86) Vilan, A.; Yaffe, O.; Biller, A.; Salomon, A.; Kahn, A.; Cahen, D. *Adv. Mater.* **2010**, *22*, 140–159.
- (87) Braun, S.; Salaneck, W. R.; Fahlman, M. *Adv. Mater.* **2009**, *21*, 1450–1472.
- (88) Fereiro, J. A.; McCreery, R. L.; Bergren, A. J. *J. Am. Chem. Soc.* **2013**, *135*, 9584–9587.
- (89) Morteza Najarian, A.; Szeto, B.; Tefashe, U. M.; McCreery, R. L. *ACS Nano* **2016**, *10*, 8918–8928.
- (90) Karipidou, Z.; Branchi, B.; Sarpasan, M.; Knorr, N.; Rodin, V.; Friederich, P.; Neumann, T.; Meded, V.; Rosselli, S.; Nelles, G.; Wenzel, W.; Rampi, M. A.; von Wrochem, F. *Adv. Mater.* **2016**, *28*, 3473–3480.
- (91) Fereiro, J. A.; Kondratenko, M.; Bergren, A. J.; McCreery, R. L. *J. Am. Chem. Soc.* **2015**, *137*, 1296–1304.
- (92) Lacroix, J. C.; Chane-Ching, K. I.; Maquère, F.; Maurel, F. *J. Am. Chem. Soc.* **2006**, *128*, 7264–7276.
- (93) Jia, C.; Migliore, A.; Xin, N.; Huang, S.; Wang, J.; Yang, Q.; Wang, S.; Chen, H.; Wang, D.; Feng, B.; Liu, Z.; Zhang, G.; Qu, D.-H.; Tian, H.; Ratner, M. A.; Xu, H. Q.; Nitzan, A.; Guo, X. *Science* **2016**, *352*, 1443–1445.
- (94) Sherif, S.; Rubio-Bollinger, G.; Pinilla-Cienfuegos, E.; Coronado, E.; Cuevas, J. C.; Agrait, N. *Nanotechnology* **2015**, *26*, 291001.
- (95) Tefashe, U. M.; Nguyen, Q. V.; Lafalet, F.; Lacroix, J. C.; McCreery, R. L. *J. Am. Chem. Soc.* **2017**, *139*, 7436–7439.
- (96) Liu, W.; Cai, S.; Deng, X. *J. Electron. Mater.* **2015**, *44*, 667–674.